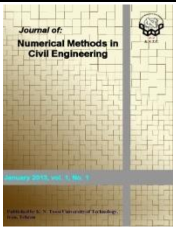

Numerical Methods in Civil Engineering

Seismic Retrofit of Vulnerable Steel Frames Using Articulated Quadrilateral bracing system

Ehsan Darvishan *

ARTICLE INFO

Article history:
Received:
August 2019.
Revised:
November 2019.
Accepted:
December 2019.

Keywords:
AQ bracing
SMA fibers
Steel Moment Frame
IDA analysis
Fragility analysis

Abstract:

This paper investigates the applicabilty of an innovative bracing, called Articulated Quadrilateral (AQ) bracing system, which uses shape memory alloys (SMAs), for retroffiting low-rise to high-rise vulnerable SMFRs against strong ground motions. The paper investigates brace fundamental engineering characteristics, design of the system and also configuration of the brace (the proportion of SMA wire, C-shape dissipator and Post-tensioning tendons). OpenSees program is utilized for nonlinear dynamic finite element analysis and the validation of modeling using data from full-scale experimental tests performed by Speicher et al. at Georgia Institute of technology. Using 3-, 9- and 20-story steel moment resisting frames from the SAC phase II project, nonlinear pushover, incremental dynamic analysis, and fragility analysis of frames with and without AQ bracing were conducted using FEMA P695 far-field ground acceleration records. Results show that by retrofitting MRF system with AQ bracing, strength of the buildings increases up to 40%. Also, bracing of the frames yields more uniform drift distribution which reduces the likelihood of soft story formation.

1. Introduction

The protection of civil structures, including material content and human occupants, is, without doubt, a worldwide priority. The extent of protection may range from reliable operation and occupant comfort to human and structural survivability. Civil structures, including existing and future buildings, towers, and bridges, must be adequately protected from a variety of incidents, including earthquakes, winds, waves, and traffic. The protection of structures is now moving from reliance entirely on the inelastic deformation of the structure to dissipate the energy of severe dynamic loadings, to the application of passive, active and semi-active structural control devices to mitigate undesired response to dynamic loads [1]. The mitigation of the hazardous effects of earthquakes begins with the consideration of the distribution of energy within a structure.

* *Corresponding Author: Assistant professor, Department of Civil Engineering, Roudehen Brach, Islamic Azad University, Roudehen, Tehran, Iran. Email: darvishan@riau.ac.ir*

During a seismic event, a finite quantity of energy is input into a structure. This input energy is transformed into both kinetic and strain energy which must be either absorbed or dissipated through heat [2].

Passive control techniques have shown to be an effective strategy when aimed at structural preservation for seismic events. These systems are designed to eliminate or at least reduce structural damage on buildings and infrastructures by limiting the transmitted displacement (Seismic Isolation techniques by causing a period shift of the structure) [3] or by absorbing the energy of the seismic event (energy dissipation techniques by providing supplemental damping) [4]. The 1970s saw the beginning of research into lead-rubber bearings (LRB) with the rubber part providing the isolation and the lead core providing damping through hysteretic behavior. Other passive devices include friction-based damper systems, such as structural bracing incorporating friction-slip elements or slotted bolted connections; viscoelastic dampers (typically installed in braces) that operate by shearing in viscoelastic material and contribute both stiffness and damping to the structure; metallic yield devices (ADAS) that dissipate energy through yielding of mild-steel plates; and viscous fluid dampers that produce a damping force proportional to some exponent of velocity [5].

One energy dissipation technique consists of using dampers based on Shape Memory Alloy (SMA) wires. Shape memory alloys have many interesting properties that can be exploited in these applications, namely; their Superelasticity, high fatigue resistance, and near strain-rate independence (in certain conditions related to temperature control), among others [6]. The shape memory effect was first discovered in 1932, but there was relatively little interest in it until 1962 when the effect was discovered in equiatomic nickel-titanium (NiTi).

Clark et al. in 1995, tested two different types of reduced-scale dampers using shape memory alloys over a range of strain amplitudes, loading frequencies, and temperatures. Parallel to the device development and testing, a series of analysis of a steel frame building incorporating shape memory alloys has been undertaken to quantify the benefits of using devices in actual structures [7]. Dolce et al. in 2000 carried out a comprehensive research in order to fully explore the possibilities of applying SMAs in the passive control of structural vibrations. Their main scope was to design the implementation, and the experimental testing of SMA-based devices for passive control of buildings, bridges and other structures [8].

Han et al. in 2005 utilized NiTi SMA wires to simultaneously damp tension, compression and torsion for structural control. The measured data revealed that the energy dissipation ratio for all tested dampers in tension, compression and torsion are in 0.33 [9].

Several studies have considered the use of SMAs as diagonal braces in frame structures [10-11]. Zhu and Zhang in 2007 compared the performance of an SMA braced frame system that employs the reusable hysteretic damper described above and buckling-restrained brace frames. They carried out nonlinear time history analysis of three-story and six-story frame buildings and found that the SMA braced frame can effectively reduce the story drifts while eliminating the residual drift problem [12].

Asgarian and Moradi investigated seismic behavior of steel frames with NiTi SMA braces. They modeled several structures with different brace configurations and compared the results with BRB frames. Results confirmed that a combination of BRB and SMA yields excellent performance [13].

Recently, a new type of bracing called Recentering Articulated Quadrilateral (AQ) bracing system, which benefits from SMA and yielding elements, is introduced. AQ system is a scalable, reconfigurable, and convenient way to combine SMA and steel wires to create an adjustable energy seismic performance. The system can maintain strength and ductility under design earthquakes. Also, it is desired for practical applications since it is easy to use and install. Experimental tests have proved its desired hysteresis behavior with adjustable amounts of energy absorption and damping [14]. However, studies on this bracing are very limited and its performance on a wide range of structures is not known.

The objective of the research presented here is to investigate the use of AQ bracing system to retrofit low-rise to high-rise steel moment resisting frames (SMRF). Three structures are selected from the SAC Phase II project: the 3-story system, the 9-story system and the 20-story system designed for the Los Angeles region. Simulation of these systems, both controlled and uncontrolled, are prepared using finite element Opensees platform with ten suites of earthquake records from FEMA P695 for far-field region.

The AQ system acts like Pall & Marsh friction damper [15], except that they used friction device to dissipate energy, but in this system, C-shape elements dissipate energy and SMA wires recenter the frame after a strong earthquake. In general, in this paper, the design of this system is explained comprehensively. Also, the proportion of SMA wire, C-shape dissipator and Post-tensioning tendons will be explained. IDA and fragility curves will then be calculated to better understand the performance of AQ system against MRF system

2. Benchmark Archetypes

In the last two decades, the seismic response of nonlinear structures to severe earthquakes has been studied and control algorithms for these nonlinear structures have been proposed by a number of researchers [16-20].

The 3-, 9- and 20-story structures used for this benchmark study were designed by Brandow & Johnston Associates for the SAC Phase II Steel Project [21]. These structures meet the seismic code and represent typical low-, medium- and high-rise buildings designed for the Los Angeles, Seattle, and Boston regions. These buildings were chosen because they also serve as benchmark structures for the SAC studies and, thus, will provide a wider basis for the comparison of results. At least two designs have been carried out for each building; one according to pre-Northridge practice and one with improved connection details according to FEMA 267 Guidelines [22] (post-Northridge designs). Basic parameters (e.g., configuration, gravity loading, etc.) are common to all locations and are believed to be representative of a great number of existing steel moment resisting frame structures. Thus, seismic evaluation of these structures provides a frame of reference for estimation of seismic demands for typical SMRF structures, and basic information for issues to be addressed in current seismic design procedures for improving the performance of new structures.

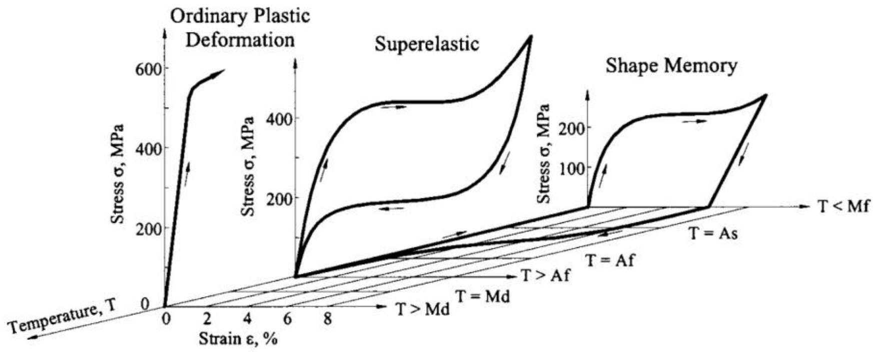

Fig. 1: Three-dimensional stress-strain temperature diagram showing deformation and SMA behavior of NiTi SMA [26]

Table 1. Typical mechanical properties of NiTi SMA compared with Structural steel [38]

	NiTi		Structural Steel	Cable Strand
	Austenite	Martensite		
Recoverable Elongation	Up to 8%		0.2%	0.42%
Young’s Modulus	30-83 GPa	21-41 GPa	200 GPa	195 GPa
Yield Strength	195-690 MPa	70-140 MPa	248-517 MPa	-
Ultimate Tensile strength	895-1900 MPa		448-827 MPa	1770-1860 MPa
Elongation at failure	5-50% (Typically ~25%)		~ 20%	~ 3.5%
Poisson’s Ratio	0.33		0.3	0

3. Shape Memory Alloy Behavior

SMAs have drawn considerable attention in the civil engineering community over the past two decades because of their unique stress-strain behavior. The combination of recentering and energy dissipation makes SMAs ideal for applications in earthquake-resistant design. In the 1990s the European Commission launched a research initiative known as the MANSIDE (Memory Alloy for New Structural Isolation Devices) project, to investigate and implement SMAs into civil engineering structures [23]. From this project, several retrofit schemes were investigated and/or developed using SMA wires and bars [8, 24, 25]. Other researchers have since investigated the mechanical properties of SMAs [26, 27] and their use in braced frames [28-30], beam-column connections [31-34], bridge deck restrainers [35], and reinforced concrete [36]. Though each of these investigations has shown varying degrees of success, limited applications have been implemented into real structures. Grasser and Cozzarelli [37] suggested the use of binary nickel-titanium (NiTi) shape memory alloys as seismic dampers.

The mechanical behavior of SMA as a function of temperature, strain, and stress is summarized in Fig. 1.

To better understand the range of behaviors observed in NiTi, a list of NiTi and steel mechanical properties are compared in Table 1.

In this paper, Structural steel elements have 200 GPa young’s modulus and 248 MPa yield strength and Cable strands have 195 GPa young’s modulus and 1860 MPa yield strength. For modeling SMA wires, a simple model proposed by Graesser and Cozzarelli [37] is adopted. This model describes the uniaxial behavior of superelastic material.

4. Bracing system behavior

In 2004, Renzi et al. [39] focused on the development of a novel dissipative bracing system based on tension-only bracing, which appears to be easier to move and to install without renouncing good performance, in particular, within light-framed structures (Fig. 2). In this study, an SMA-based recentering system is used [23]. This system provides both recentering and damping in a scalable arrangement. Driven by SMA’s unique ability to recover strains of up to approximately 8% through a diffusionless phase transformation, the cornerstone of the bracing proposed herein, is the ability to adjust the energy dissipation in a recentering hysteretic loop through the use of an AQ arrangement. SMA wire bundles are installed within the AQ, where the system acts like Pall & Marsh friction damper, except, they used friction device to dissipate energy. But, in this system, C-shape elements dissipate energy and SMA wires recenter the frame after a strong earthquake. A schematic of the loading frame and the AQ is shown in Fig. 3. As seen in Fig. 3, columns are attached to beams with hinge connections, which means the frame has no lateral stiffness and the lateral stiffness comes from the bracing system.

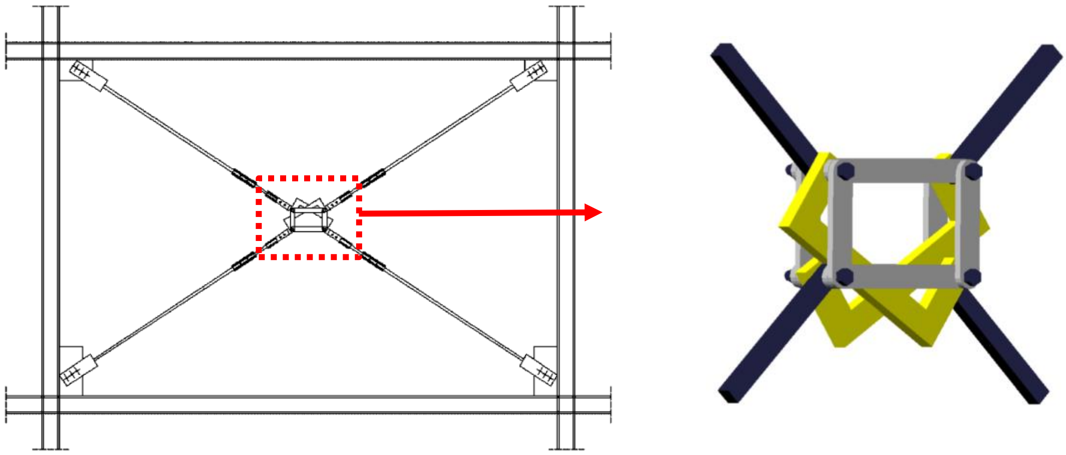

Fig. 2: C-shape dissipator in AQ [40]

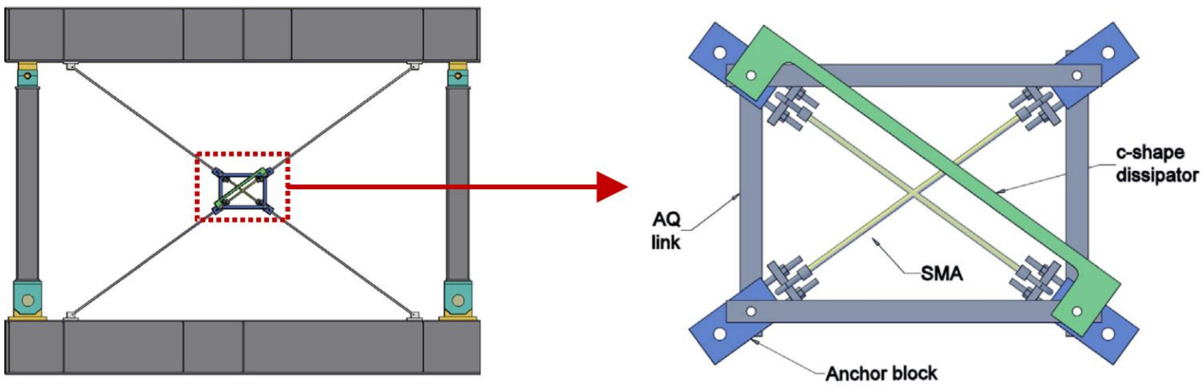

Fig. 3: general AQ setup with SMA and C-shape element [23]

As indicated in Renzi, while small drifts do not induce axial force due to the kinematic behavior of the AQ, for large displacements, the diagonal which becomes shorter varies its length more than the other one and so the entire bracing system is stretched. This behavior indicates that this type of retrofitting does not affect stiffness of the structural frame and becomes activated when the beams forms plastic hinge in them. For addressing this issue, the frame should be simple with no lateral stiffness (beam-column connection should be simple).

Due to their shapes, the C-shape dissipators act as bending elements and SMA wires act as axial elements. However, SMA wires and Cable strands have pretention forces when implanted because they shouldn't act as compression elements. This pretension force holds them in tension mode for some time during an earthquake.

C-shape dissipators do not always yield by bending moment. Nevertheless, based on their slenderness $\left(\frac{b}{h}\right)$, they can either yield or buckle by axial forces. Based on numerical analysis, there is no constant $\frac{b}{h}$ above it, where yielding by bending can be set apart from yielding or buckling under axial force. b and h are the width and height of C-shape element, respectively. But after $\left(\frac{b}{h}\right) < \frac{1}{6}$ the difference becomes more evident. It's better to choose a C-shape element with $\left(\frac{b}{h}\right) > \frac{1}{6}$. In that case, the equations of stiffness and strength which are shown in the next pages are validated. Height of C-shape element (h) also affects the stiffness and strength of it. For better results, h should be less than 6 in.

The SMA wires and C-shape elements work in parallel with each other. It means that the stiffness and the strength of the bracing system are the sum of the stiffness of both of them.

Because of the unique shape of C element, its stiffness has an unique equation as presented shown in equation (1) and its strength is like a bending beam, as shown in equation (2).

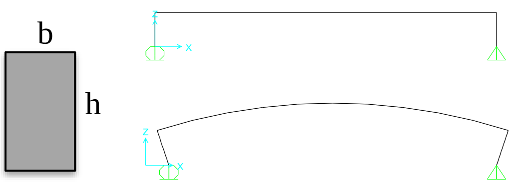

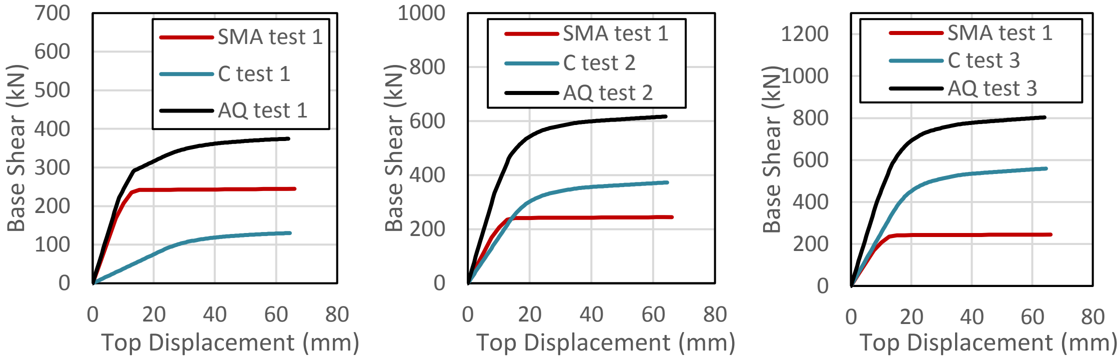

(a) (b) (c)

Fig. 4: The bracing system pushover behavior when: (a) at condition b; (b) at condition b; and (c) at condition c

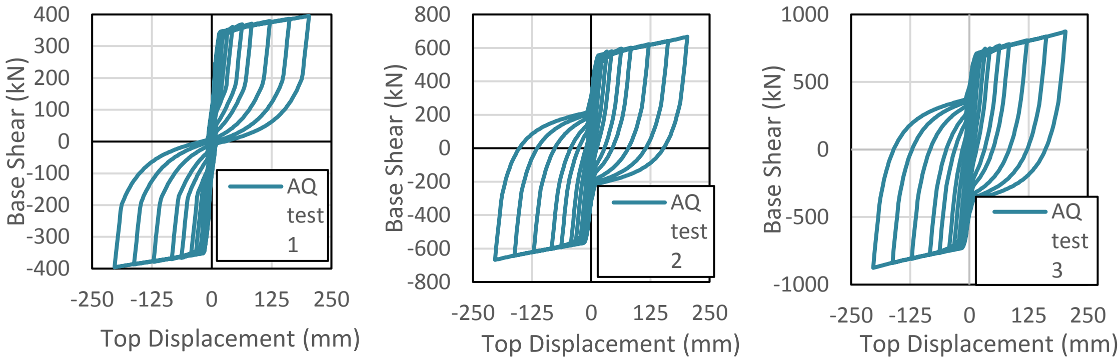

(a) (b) (c)

Fig. 5: The bracing system cyclic behavior when: (a) at condition a; (b) at condition b; and (c) at condition c

$$\begin{cases} K_{C-shape} = b.(0.23h^3 + 0.04h^2 - 0.07h + 0.037) \\ h \leq 6 \end{cases} \quad (1)$$

$$M_{C-shape} = Z.f_y \quad (2)$$

If this C-shape element is used in AQ bracing, because it tilted and doubled (Fig. 2), the AQ bracing stiffness is $2(\cos)^2\,\theta$ times the stiffness of C-shape. θ is the angle of C-shape in AQ bracing from horizontal axes.

The SMA wires have pretension force, which means, when AQ bracing deforms, both of them act against it until pretension force becomes zero. From that moment only one of them acts against lateral load until the brace yields. This behavior forms three line curve of AQ bracing behavior with only SMA wires.

The yielding force of the bracing system is divided into two-phases because yielding of the C-shape element and SMA wire does not occur at the same time and depends on their stiffness and yielding stress. Three conditions have been investigated: a) SMA wires have more strength and stiffness than C-shapes; b) SMA wires have more stiffness but less strength than C-shapes; and c) SMA wires have less strength and stiffness than C-shapes. The pushover curve of each element and AQ bracing is depicted in Fig. 4 and the cyclic behavior of AQ bracing in Fig. 5. SAC far field cyclic loading protocol [41] was used for cyclic loading. If the designer wants to have full self-centering system, these behaviors prompt C-shape element which is weaker than SMA wires. In this paper full self-centering behavior has been chosen.

The effect of pretensioning force in SMA wires and Cable strands to other structural elements have been investigated (Fig. 6). Results shows that P1 (pre-tensioning force in SMA) develops negative moment in C-shapes but P2 (pre-tensioning force in Cable) develops positive moment in C-shapes. Hence, when both SMA wire and Cable strand have pre-tensioning force, moment developed in C-shape will be less than when one of them has pre-tensioning force. Results show that the moment developed in C-shapes in comparison with pretensioning force is ignorable.

The deformed shape of AQ bracing is shown in Fig. 7. The dashed line and continuous line represents undeformed and deformed shape of the frame, respectively. This deformation is when C-shape elements bent (from bending moment) and SMA wire yielded (from axial force). The general strategy is to concentrate the inelastic deformations into SMA and C-shape only: thus the remainder of the frame should remain completely elastic. Cables have pretension force and therefore do not buckle. Cables numbers (1) and (3) are in compression mode,

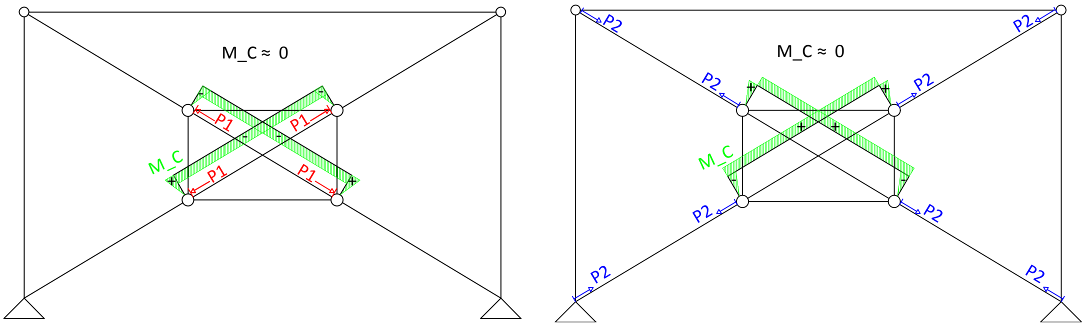

(a) (b)

Fig. 6: Effect of pretension force on C-shape moment: (a) SMA wires; (b) cable tendons

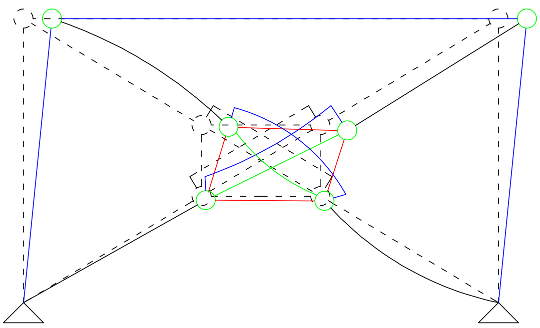

Fig. 7: AQ bracing frame: deformed shape under external force

which means after certain displacement of frame, they buckle and do not tolerate forces anymore. Cables number (2) and (4) are in tension mode. Also one of the SMA wires which is in the compression mode buckles, and does not affect the frame behavior.

5. Bracing system design

Since the AQ brace is newly introduced, there is no exclusive design procedure for it. In this study, we employed Renzi et al. and Ciampi et al. [42] approach to design the braces.

Based on Renzi et al. work, there are two design parameters:

$$\lambda = {}^{K_b}\!/_{K_f} \qquad (3)$$

$$\eta_b = {}^{F_{by}}\!/_{m.\ddot{u}_{G,max}} \qquad (4)$$

Where, m is the structural mass, K_f is the frame (MRF system) stiffness, K_b, and F_{by} represent stiffness and yielding force of the bracing system (just AQ system) respectively, and $\ddot{u}_{G,max}$ is the maximum ground acceleration used in the response analysis. The value of λ is considered to vary between 0 and 10; the value of 0 represents the unbraced frame case, while the value of 10 represents a realistic upper limit for the relative stiffness of the bracing.

In Ciampi et al. paper, there are three more parameters including:

$$\eta_f = {}^{F_{fy}}\!/_{m.\ddot{u}_{G,max}} \qquad (5)$$

$$\beta = {}^{\delta_{by}}\!/_{\delta_{fy}} \qquad (6)$$

$$\mu_f = {}^{\delta_{max}}\!/_{\delta_{fy}} \qquad (7)$$

Where F_{fy} represents yielding force of the MRF system, β is the ratio between the displacement which causes yielding in the brace and the corresponding yielding displacement of the frame, and μ_f is maximum frame ductility. The value of β has been made variable only between 0 and 1; the limit case β = 0 corresponds to having no bracing; the other limit case β = 1 corresponds to the situation where the bracing and frame yield for the same displacement.

The above equations are for single DOF frames, but for multi DOF frames, we followed 'local' approach [42]. The 'local' approach consists of selecting the parameters of the bracings at each level, F_{byi} and K_{bi}, for assigned distributions of frame stiffness and strengths, according to the following local relations:

$$\eta_{bi} = \beta\lambda\eta_{fi} \quad , \quad K_{bi} = K_{fi} \qquad (8)$$

The design procedure is: First stiffness (K_{fi}), strength (η_{fi}) and corresponding yield displacement (δ_{fy}) of the unbraced frame is calculated. Then, by assuming λ and β, stiffness (K_{bi}) and strength (η_{bi}) of the bracing system is calculated.

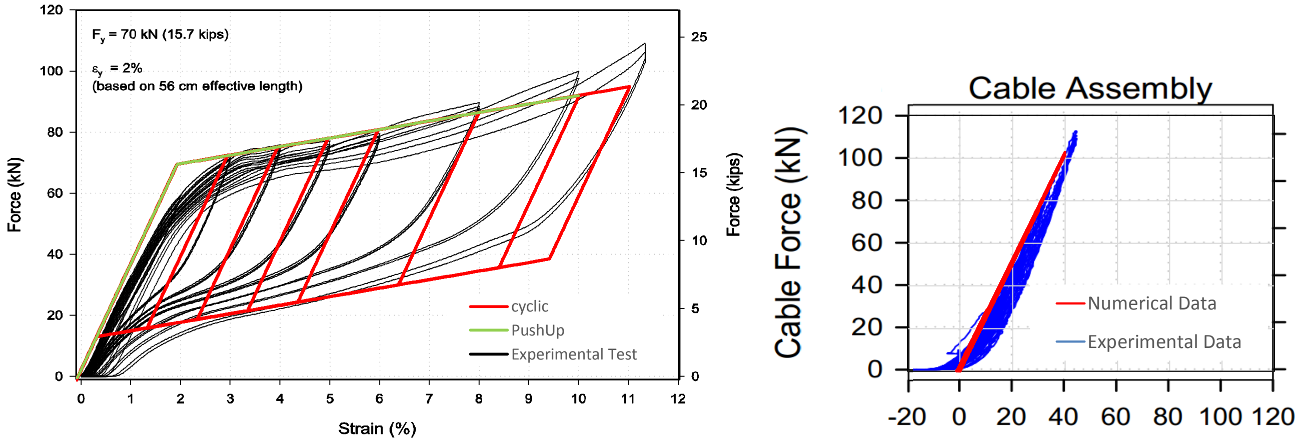

(a) (b)

Fig. 8: (a) Force-Strain curve of NiTi SMA Wire; (b) Force-displacement of tendons

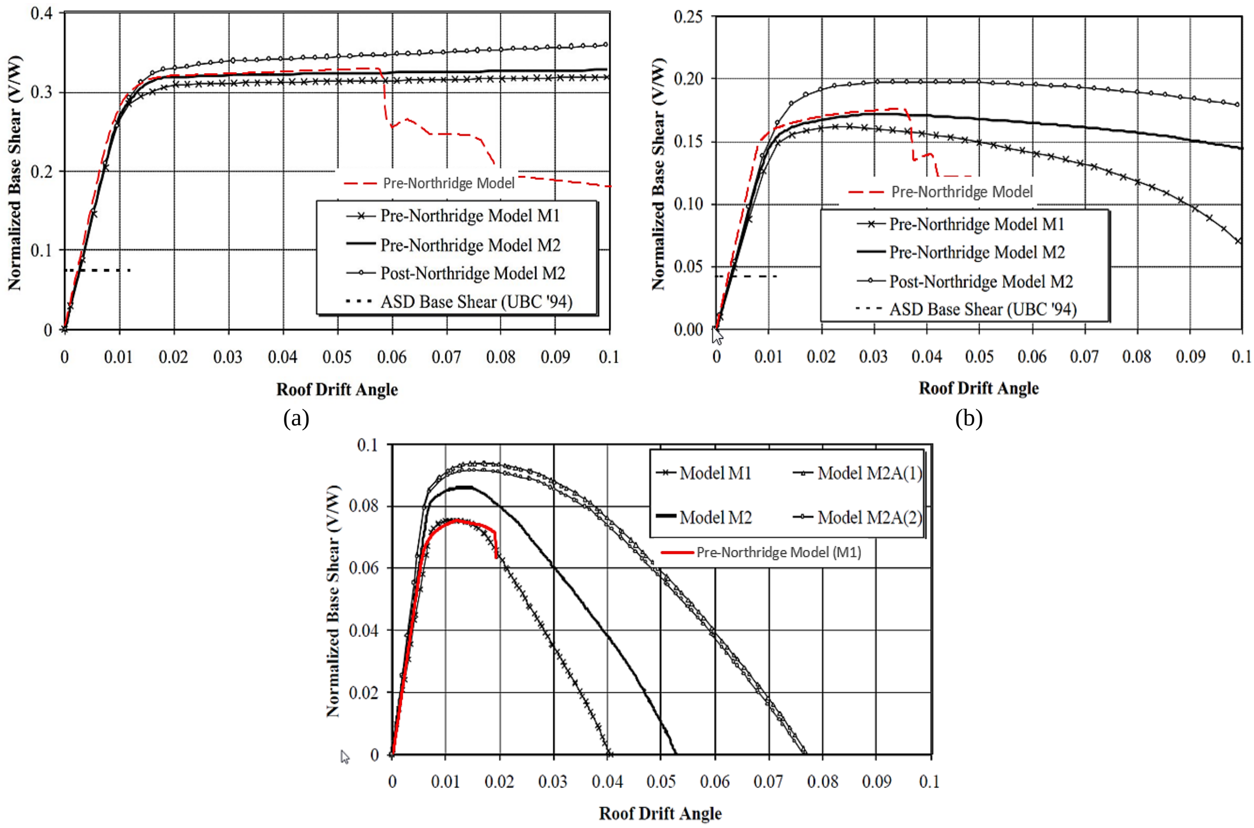

(a) (b) (c)

Fig. 9: Pushover curve of the buildings: (a) 3-story, (b) 9-story and (c) 20-story

In this study, λ and β are taken as 1 and 0.5, respectively. Therefore, $K_{bi} = K_{fi}$ and $\eta_{bi} = 0.5\eta_{fi}$ in each story of the frame. $K_{fi}, \eta_{fi}, \delta_{fy}$ of the frame are listed in Table 3. Also, design parameters of braces are listed in Table 4.

6. Validation

This section discusses the analytical model of the AQ braces which is calibrated using the test results from Speicher et al. [23]. This analytical model will be used to simulate the hysteretic behavior of AQ brace in the nonlinear time-history analysis of MRFs presented in the next section. Fig. 8(b).

Further data about the experimental test can be found in Speicher et al. A constitutive law which describes the stress-strain relationship of SMAs is a necessity to a numerical simulation study. A modified version of the constitutive model of SMA was initially developed by Grasser and Cozzarelli. The Grasser and Cozzarelli model was later extended by Wilde et al. [43] to include the hardening behavior of SMA material after the transition from the austenite to martensite is completed.

Table 2. Parameters of SelfCentering Material

K1 (KN/mm)	K2 (KN/mm)	SigAct (KN)	beta	eps slip	epsBear	rBear
66.03	5.28	70	0.8	0.0	0.0	0.02

Table 3. Stiffness and strength of MRF system

Stories	3-story building			9-story building			20-story building		
	Initial stiffness (kN/mm)	Strength (kN)	δ_{fy} (mm)	Initial stiffness (kN/mm)	Strength (kN)	δ_{fy} (mm)	Initial stiffness (kN/mm)	Strength (kN)	δ_{fy} (mm)
Story 1	182	5542	30	131	8629	66	0	0	0
Story 2	174	6596	38	334	13388	41	300	11747	43
Story 3	111	3634	33	308	11663	38	310	11480	41
Story 4				296	11876	41	311	11471	41
Story 5				250	9474	38	312	11476	41
Story 6				243	9652	41	261	8723	41
Story 7				175	6672	38	248	8731	41
Story 8				148	6716	46	248	8758	41
Story 9				110	4448	41	249	8780	41
Story 10							249	8780	41
Story 11							249	8780	41
Story 12							249	8780	41
Story 13							249	8780	41
Story 14							249	8780	41
Story 15							249	8780	41
Story 16							249	8780	41
Story 17							249	8780	41
Story 18							249	8780	41
Story 19							117	4715	36
Story 20							102	3403	36

Table 4. Design parameters of AQ brace

Stories	3-story building			9-story building			20-story building		
	Initial stiffness (kN/mm)	post-activation stiffness (kN/mm)	δ_{by} (mm)	Initial stiffness (kN/mm)	post-activation stiffness (kN/mm)	δ_{by} (mm)	Initial stiffness (kN/mm)	post-activation stiffness (kN/mm)	δ_{by} (mm)
Story 1	182	14.54	15	131	10.48	33	0	0	0
Story 2	174	13.92	19	334	26.72	20.5	300	24	21.5
Story 3	111	8.88	16.5	308	24.64	19	310	24.8	20.5
Story 4				296	23.68	20.5	311	24.88	20.5
Story 5				250	20	19	312	24.96	20.5
Story 6				243	19.44	20.5	261	20.88	20.5
Story 7				175	14	19	248	19.84	20.5
Story 8				148	11.84	23	248	19.84	20.5
Story 9				110	8.8	20.5	249	19.92	20.5
Story 10							249	19.92	20.5
Story 11							249	19.92	20.5
Story 12							249	19.92	20.5
Story 13							249	19.92	20.5
Story 14							249	19.92	20.5
Story 15							249	19.92	20.5
Story 16							249	19.92	20.5
Story 17							249	19.92	20.5
Story 18							249	19.92	20.5
Story 19							117	9.36	18
Story 20							102	8.16	18

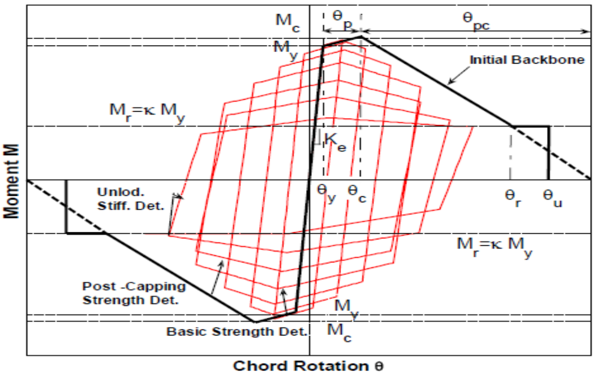

Fig. 10: Parameters of hysteresis curves of W sections [49]

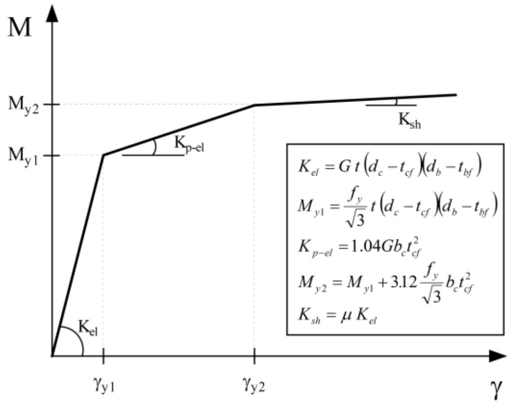

Fig. 11: Krawinkler panel zone parameters [21]

The material used for modeling the SMA wires in this paper in OpenSees platform is SelfCentering Material. This material is primarily used to model a self-centering energy dissipative brace [44]. Fig. 1(a) shows the force-strain relationship of superelastic NiTi wires from the experimental data and the SelfCentering Material, respectively. Parameters of SelfCentering Material used in this study are depicted in Table 2. Since SMA wires buckle in compression, they are modeled as tension-only materials. A nonlinear truss element is used to model SMA wires. Fig. 8(a) shows verification of the SMA wires. The black lines are taken from experimental study by Miller [45] and the red lines show the modelling results in this study.

The post-tensioning strands are modelled by a bilinear constitutive relationship. Steel4 Material is employed in Opensees which accounts for post-tensioning force in strands. The young modulus, yield stress, and post-tensioning of tendons are 200 GPa, 1750 MPa, and 175 MPa, respectively. Again, nonlinear truss element is used to model tendons. Fig. 8(b) shows the results of verification of tendons. In this figure, black lines are taken from experimental study by Renzi et al. [39] and the red lines are obtained by the analytical modelling in this study.

7. Buildings design

In this paper, AQ brace is designed for each structure separately. For designing the elements of the AQ bracing system including pretension tendons, AQ links, SMA wires and C-shape dissipators, first the stiffness of MRF system should be calculated, then λ and η should be assumed and after subsequently, the stiffness and strength of the bracing system can be calculated. The stiffness of MRF system is equal to the initial slope of its pushover curve. The verification of pushover curves of the 3-story, 9-story and 20-story MRF frames are shown in Fig. 9. In this figure, black lines are taken from the study reported in FEMA 355C [46] and the red lines are pushover curves obtained from this study. The 3-story and 9-story buildings are modeled with panelZone (Model M2 in pushover curve) but the 20-story building is modeled without panelZone (Model M1) for faster analysis. As shown, they matched very well, but our models have stiffness and strength reduction defined in elements behavior, so they collapse after certain displacement.

Design procedure of AQ frame elements including (cables, C-shapes and SMA wires) is shown in

Table **2.** Parameters of SelfCentering Material

K1 (KN/mm)	K2 (KN/mm)	SigAct (KN)	beta	epsslip	epsBear	rBear
66.03	5.28	70	0.8	0.0	0.0	0.02

Table . By calculating every story stiffness, and assuming λ, the stiffness of AQ frame can be estimated. As mentioned earlier, to achieve full recycling behavior, SMA wires should possess more strength and stiffness than C-shapes. C-shape element and SMA wires work in parallel. Therefore, the stiffness of the brace is equal to the sum of the stiffness of C-shape element and SMA wires. In this study, stiffness of the C-shape elements are considered as 0.7 of the stiffness of the brace for all stories. Also, post-elastic strength of the C-shape element is assumed to be 0.8 of the SMA wire.

8. Analyitical models

Individual analytical models for the 3-, 9- and 20-story frames with and without retrofitting devices are developed as two-dimensional frames in the Open System for Earthquake Simulation (OpenSees) [47]. Based on the concentrated plasticity concept, the beam and column elements are modeled with elastic beam-column elements connected by zero-length inelastic plastic hinges employing the modified Ibarra-Krawinkler deterioration model [48]. The modified Ibarra-Krawinkler deterioration model considers bilinear hysteretic response behavior. The cyclic deterioration parameters of the zero-length rotational springs are assigned based on the model parameters developed by Lignos and Lrawinkler [49]. The deterioration characteristics of the rotational springs are indicated by yield strength, post-capping strength, unloading stiffness, and reloading stiffness. The moment-rotation curve is characterized by the elastic stiffness, plastic rotation, a post-capping plastic rotation capacity and the corresponding residual strength (Fig. 10). The used connection parameters are based on the values of Eq. (8) recommended by Lignos and Lrawinkler.

$$\theta_p = 0.07.(\frac{h}{t_w})^{-0.35}.(\frac{b_f}{2t_f})^{-0.31}.(\frac{d}{c^1_{unit}.21"})^{-0.281}.(\frac{C^2_{unit}.F_y}{50})^{-0.383} \quad (8)$$

$$\Lambda = \frac{E_t}{M_y} = 26.36.(\frac{h}{t_w})^{-0.589}(\frac{b_f}{2t_f})^{-0.574}.(\frac{c^2_{unit}F_y}{50})^{-1.545}$$

$$\theta_{pc} = 4.645.(\frac{h}{t_w})^{-0.449}.(\frac{b_f}{2t_f})^{-0.837}.(\frac{d}{c^1_{unit}.21"})^{-0.265}$$

$$.(\frac{C^2_{unit}.F_y}{50})^{-1.136}$$

Where $h, t_w, t_f, b_f, F_y, L, d, C^1_{unit}, C^2_{unit}, \Lambda$, are depth and width of web, depth and width of flange, yield stress, bay length, beam depth, and constant values, respectively. To capture the important panel zone deformation modes, the panel zones are modeled considering the shear distortion in beam-column joints using Krawinkler model [21]. The parameters of the three-linear Krawinkler curve are shown in Fig. 11. In this figure, indices of b and c denote beam and column, and *w* and *f* denote web and flange.
The nonlinear plastic hinges are created in beams at an offset from the interface of the panel zone and the column element. To account for P-delta effects, a leaning column is linked to each model with elastic beam-column elements and connected to the model with an axially rigid truss element at each story level [48] (Fig. 12 and 13). The model assumes Rayleigh damping with a 5% damping ratio for the first and third modes.
The AQ links were made from 12.7 mm thick, 50.8 mm wide A36 flat bar. The joints were pinned. The dimension of the AQ was governed by the dimensions of the loading frame (height-to-width ratio kept the same). The cable assemblies that connected AQ to the loading frame were made up of 25.4 mm 18-7 bright wire cable with thimbles and swag sleeves at each end.
Based on ground motion characteristics for example, the sites of records located greater than or equal to 10 km from the fault rupture and have moment magnitudes (M_w), peak ground acceleration (PGAs) and peak ground velocities (PGVs) of higher than 6.5 and 0.2 g and 15 cm/s, respectively. The collapse limit state for each archetype frame was considered as the time in which the maximum story-drift ratio exceeds 10% according to Vamvatsikos and Cornell.
Because analytical model is in 2D, the direction of each earthquake had been chosen to have bigger PGA. The first analytical period is presented in Table .
Fig. shows the IDA curves for the 3-, 9-, and 20-stories SAC buildings with and without retrofitting device, which are plotted in terms of two efficient and sufficient parameters, including maximum inter-story drift ratio and PGA.

9. Nonlinear static analysis

To evaluate the performance of AQ bracing system, and compare it to the traditional MRF system, first, the pushover analysis had been conducted. Results compare stiffness, strength, and ductility of the systems. As shown in Fig. 14, both of the systems have the same stiffness because this type of retrofit does not affect stiffness. However, AQ bracing system has more strength and ductility than MRF system. Strength and stiffness reduction on both of the systems occurs because of reduction of stiffness in beams.
Fig. 14 shows pushover curve of the structures. Both MRF systems have more strength at yield point than AQ bracing system, but the hardening stiffness of AQ bracing system is bigger than MRF system. Also in 20-story building because of P-Delta effect, hardening stiffness is negative.

10. Nonlinear incremental dynamic analysis

Static pushover analysis is not enough to assess the behavior of AQ bracing system. To assess the validity of the proposed retrofitting system for these buildings, it is necessary to perform Incremental Dynamic Analysis (IDA) [50]. IDA is an analytical method for estimating the distribution of demand and capacity of the structure under predefined multiply scaled records, in which a series of nonlinear dynamic analyses are performed from low to collapse intensities [51]. IDA curves of the structural response, as measured by a damage measure (DM, e.g., peak roof drift ratio θ_{roof} or θ_{max}), versus the ground motion intensity level measured by a damage measure (DM, e.g., peak ground acceleration, PGA, or the 5% damped first-mode spectral acceleration $S_a(T_1,5\%)$) can be generated. In this paper, 200 nonlinear dynamic analyses for each model (1200 in total), including 10 records scaled from 0.1 to 2 g by the 0.1 g step, are carried out. The DM and IM used are θ_{max} and PGA, respectively. IDA is carried out using far-field ground motion set, adopted from FEMA P695 [52]. The records are listed in Table A1, Appendix A.

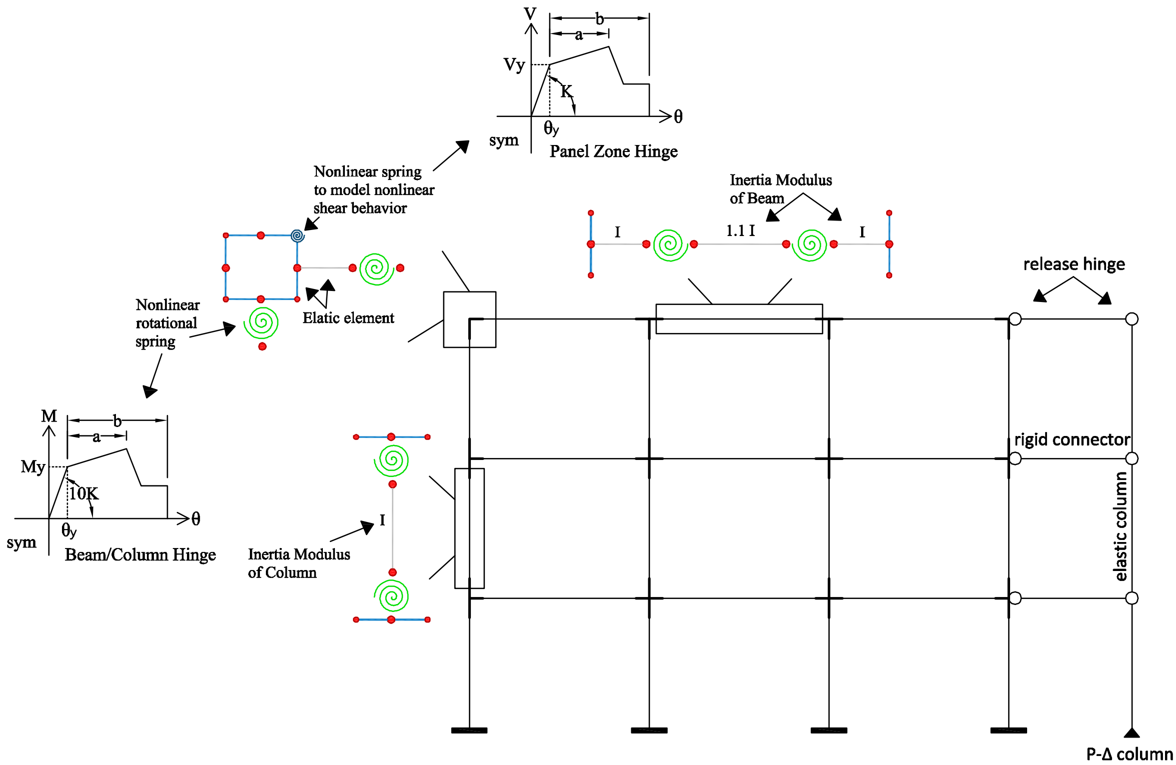

Fig. 12: An analytical model of the 3-story SAC building

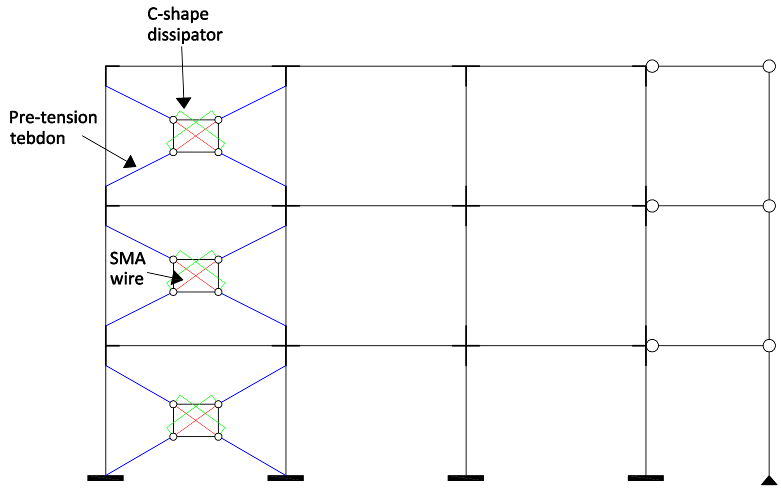

Fig. 13: An analytical model of the 3-story Retrofitted building

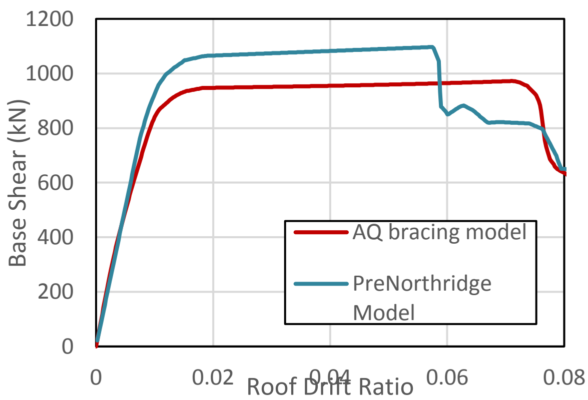

(a)

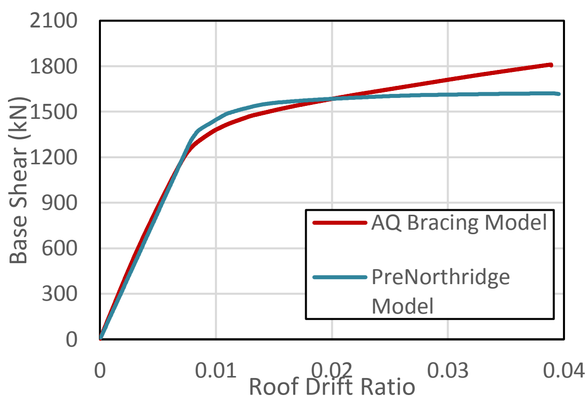

(b)

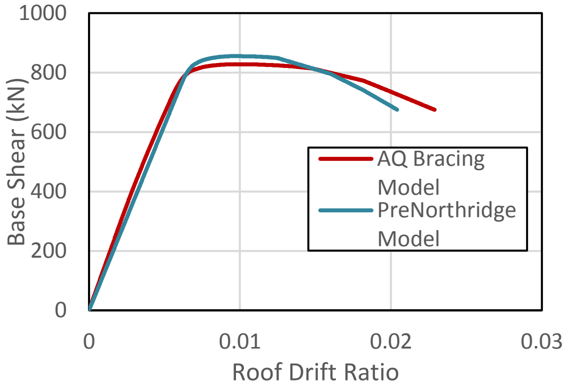

(c)

Fig. 14: Pushover curve for MRF and Retrofitted model (a) 3-story building (b) 9-story building (c) 20-story building

Table 5. Analytical period of models

Model	3-story	9-story	20-story
period	1.00	2.36	4.26

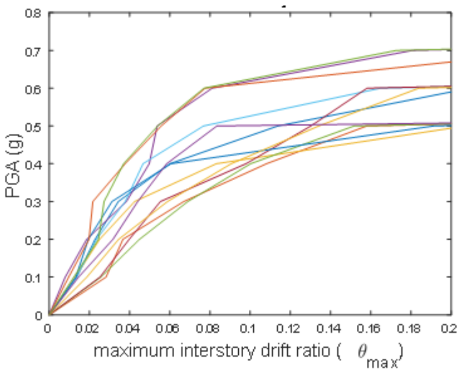

(a)

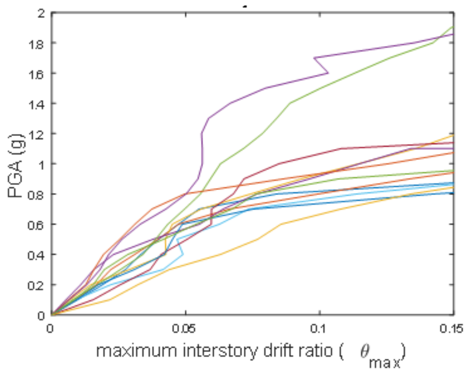

(b)

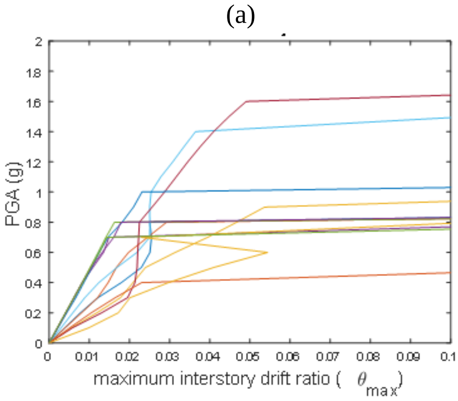

(c)

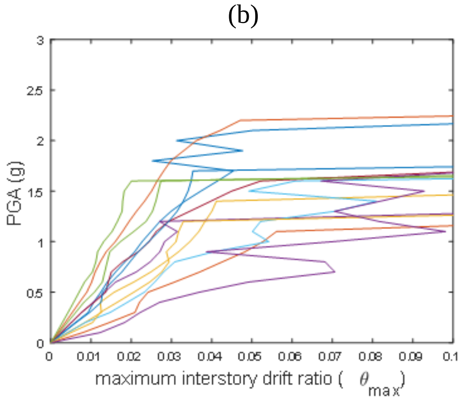

(d)

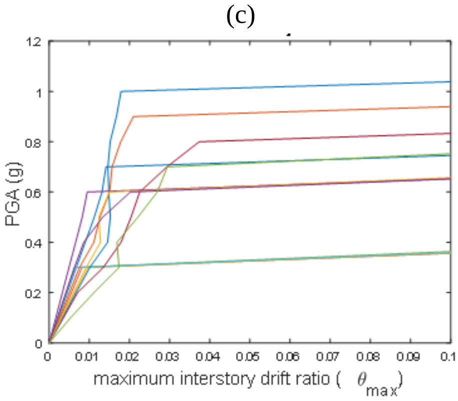

(e)

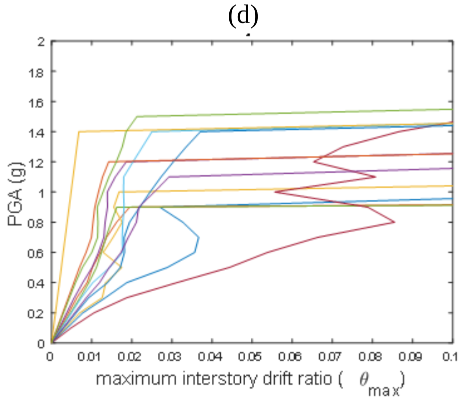

(f)

Fig. 15: IDA curve of (a) 3-story MRF (b) 3-story AQ (c) 9-story MRF (d) 9-story AQ (e) 20-story MRF (f) 20-story AQ (c)

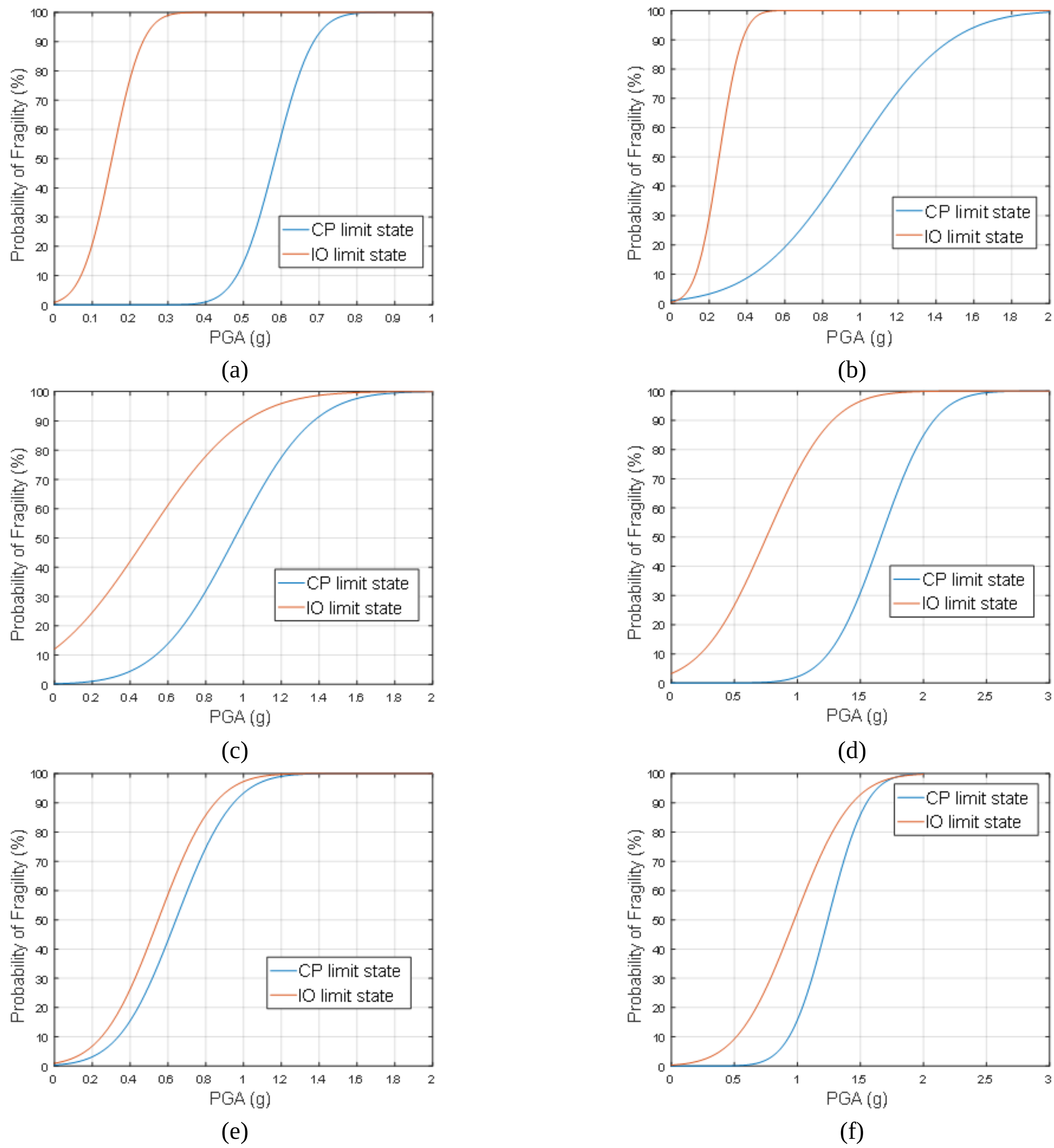

Fig. 16: Fragility curves of (a) 3-story MRF (b) 3-story AQ (c) 9-story MRF (d) 9-story AQ (e) 20-story MRF (f) 20-story AQ (c)

Fig. 15 shows the IDA curves of the buildings with and without bracing. Results from IDA curves shows that buildings retrofitted with AQ bracing need a stronger earthquake (about 40% more) to collapse.

11. Discussion

An important issue in performance-based earthquake engineering (PBEE) is the estimation of structural performance under seismic loads, in particular the estimation of the mean annual frequency (MAF) of exceeding a specific level of structural demand (e.g., the maximum, over all stories, peak interstory drift ratio θ_{max}) or a certain limit-state capacity (e.g., global dynamic instability) [53]. In order to be able to carry out the performance calculations needed for PBEE, we need to define limit-states on the IDA curves. For our case study, we chose to demonstrate two: immediate occupancy (IO), and collapse prevention (CP) both defined in SAC [54, 55]. For a steel moment-resisting frame, IO is violated at $\theta_{max} = 2\%$, according to SAC [54]. On the other hand, CP is not exceeded on the IDA curve until the final point where the local tangent reaches 20% of the elastic slope or $\theta_{max} = 10\%$, whichever occurs first in IM terms.

Using collapse data from IDA results, a collapse fragility curve can be defined through a cumulative distribution function (CDF), which relates the ground motion intensity to the probability of collapse [56]. Fig. 16 shows cumulative distribution plot obtained by fitting a lognormal distribution to the IO and CP data. As seen, by increasing the height of the buildings, probability of fragility for IO and CP limit states become closer and in 20-story building, the CP and IO limit state occur together, which means that if the building reaches IO limit state, it collapses.

Also, the figure shows that the 50 percent probability of reaching IO limit state for 3-, 9- and 20-story MRF buildings are 0.6, 0.9 and 0.7 g respectively, and the 50 percent probability of reaching IO limit state for 3-, 9- and 20-story AQ bracing buildings are 1.0, 1.3 and 1.24 g respectively. As seen, in IO limit state, by increasing the height of the buildings, the acceleration that reaches the building to IO limit state increases, but in CP limit state, the acceleration that reaches the building to CP limit state decreases by increasing the height of the building.

12. Conclusion

The behavior of a SMA-based bracing system is largely governed by the stiffness of the attributing parts. The general strategy is to concentrate the inelastic deformations only into the SMA: thus the remainder of the brace should remain completely elastic. The relative stiffness of the SMA elements and those which are in series with the SMA elements (steel cables and C-shapes) are important. The adjacent elements should be made stiffer than that of the SMA in order to get full advantage of the SMA loading plateau. An analytical study demonstrated that the SMA bracing system had the best performance in terms of inter-story drift. These SMA systems tended to distribute the drifts move evenly over the height of the structure, thus reducing the likelihood of the formation of soft stories. Additionally, the SMA systems shows more strength in IDA results.

It is notable that although this brace shows superior performance, it has some limitations. When displacements of the structure pass a certain value, the pretension forces disappear and half of the cables fail. This adversely affects the performance of the brace. Also, cost of the SMA wires is another issue that must be solved for practical applications.

References

[1] Lotfollahi, M., & Alinia, M. M., Effect of tension bracing on the collapse mechanism of steel moment frames, Journal of Constructional Steel Research, 2009, 65(10-11): p. 2027-2039.

[2] Soong, T.T. and M.C. Costantinou, *Passive and active structural vibration control in civil engineering*. 345. p. 2014: Springer.

[3] Weisman, J. and G.P. Warn, *Stability of elastomeric and lead-rubber seismic isolation bearings.* Journal of Structural Engineering, 2011. 138(2): p. 215-223.

[4] Veismoradi, S., Cheraghi A., and Darvishan, E., Probabilistic mainshock-aftershock collapse risk assessment of buckling restrained braced frames, Soil Dynamics and Earthquake Engineering, 2018. 115: p. 205-216.

[5] Wilson, J.C. and M.J. Wesolowsky, *Shape Memory Alloys for Seismic Response Modification: A State-of-the-Art Review.* Earthquake Spectra, 2005. 21(2): p. 569-601.

[6] Dolce, M. and D. Cardone, *Mechanical behaviour of shape memory alloys for seismic applications 1. Martensite and austenite NiTi bars subjected to torsion.* International Journal of Mechanical Sciences, 2001. 43(11): p. 2631-2656.

[7] Clark, P.W., et al., *Experimental and analytical studies of shape-memory alloy dampers for structural control*. Smart Structures and Materials '95. Vol. 2445. 1995: SPIE.

[8] Dolce, M., D. Cardone, and R. Marnetto, *Implementation and testing of passive control devices based on shape memory alloys.* Earthquake Engineering & Structural Dynamics, 2000. 29(7): p. 945-968.

[9] Han, Y.-L., et al., *NiTi-wire Shape Memory Alloy Dampers to Simultaneously Damp Tension, Compression, and Torsion.* Journal of Vibration and Control, 2005. 11(8): p. 1067-1084.

[10] Saadat, S., et al., *Using NiTi SMA tendons for vibration control of coastal structures.* Smart Materials and Structures, 2001. 10(4): p. 695.[**11]** Moradi, S., Alam, M. S., & Asgarian, B. Incremental dynamic analysis of steel frames equipped with NiTi shape memory alloy braces. The Structural Design of Tall and Special Buildings, 2014, 23(18), p. 1406-1425.

[12] Zhu, S., & Zhang, Y. (2007). Seismic behaviour of self-centring braced frame buildings with reusable hysteretic damping brace. Earthquake engineering & structural dynamics, 36(10), p. 1329-1346.

[13] Asgarian, B., & Moradi, S. Seismic response of steel braced frames with shape memory alloy braces. Journal of Constructional Steel Research, 2011, 67(1), p. 65-74.

[14] Speicher MS, DesRoches R, Leon RT. Cyclic Testing of a SMA-Based Articulated Quadrilateral Bracing System. InThe International Conference on Shape Memory and Superelastic Technologies 2010.

[15] Pall, A.S. and C. Marsh, *Response of friction damped braced frames.* Journal of Structural Engineering, 1982. 108(9): p. 1313-1323.

[16] Bekey, G. and T. Oaughey, *On-line control of nonlinear flexible structures.* Journal of Applied Mechanics, 1982. 49: p. 877.

[17] Reinhorn, A., G. Manolis, and C. Wen, *Active control of inelastic structures.* Journal of engineering mechanics, 1987. 113(3): p. 315-333.

[18] Yang, J., Z. Li, and S. Liu, *Control of hysteretic system using velocity and acceleration feedbacks.* Journal of engineering mechanics, 1992. 118(11): p. 2227-2245.

[19] Yang, J., Z. Li, and S. Vongchavalitkul, *Generalization of optimal control theory: linear and nonlinear control.* Journal of engineering mechanics, 1994. 120(2): p. 266-283.

[20] Barroso, L.R. and H.A. Smith, *Performance evaluation of vibration controlled steel structures under seismic loading*. 1999: John A. Blume Earthquake Engineering Center.

[21] Gupta, A. and Krawinkler H., *Seismic demands for the performance evaluation of steel moment resisting frame structures*. 1999, Stanford University Stanford, California.

[22] Venture, S.J., *Interim guidelines: evaluation, repair, modification and design of steel moment frames.* Rep. No. SAC 95, 1995.

[23] Speicher, M.S., R. DesRoches, and R.T. Leon, *Investigation of an articulated quadrilateral bracing system utilizing shape*

memory alloys. Journal of Constructional Steel Research, 2017. 130: p. 65-78.
[24] Dolce, M. and D. Cardone, *Theoretical and Experimental Studies for the Application of Shape Memory Alloys in Civil Engineering.* Journal of Engineering Materials and Technology, 2006. 128(3): p. 302-311.
[25] Dolce, M., D. Cardone, and R. Marnetto. *SMA re-centering devices for seismic isolation of civil structures*. in *Proceedings of SPIE*. 2001.
[26] DesRoches, R., J. McCormick, and M. Delemont, *Cyclic properties of superelastic shape memory alloy wires and bars.* Journal of Structural Engineering, 2004. 130(1): p. 38-46.
[27] McCormick, J., et al., *Structural engineering with NiTi. II: mechanical behavior and scaling.* Journal of Engineering Mechanics, 2007. 133(9): p. 1019-1029.
[28] Zhu, S. and Y. Zhang, *Seismic analysis of concentrically braced frame systems with self-centering friction damping braces.* Journal of Structural Engineering, 2008. 134(1): p. 121-131.
[29] Speicher, M., et al., *Shape memory alloy tension/compression device for seismic retrofit of buildings.* Journal of Materials Engineering and Performance, 2009. 18(5-6): p. 746-753.
[30] Miller, D.J., L.A. Fahnestock, and M.R. Eatherton, *Development and experimental validation of a nickel–titanium shape memory alloy self-centering buckling-restrained brace.* Engineering Structures, 2012. 40: p. 288-298.
[31] Ocel, J., et al. *Full-scale testing of nitinol based semi-rigid connections*. in *Proceedings of the 12th European Conference on Earthquake Engineering*. 2002.
[32] Sepúlveda, J., et al., *Steel beam–column connection using copper-based shape memory alloy dampers.* Journal of Constructional Steel Research, 2008. 64(4): p. 429-435.
[33] DesRoches, R., B. Taftali, and B.R. Ellingwood, *Seismic performance assessment of steel frames with shape memory alloy connections. Part I—analysis and seismic demands.* Journal of Earthquake Engineering, 2010. 14(4): p. 471-486.
[34] Ellingwood, B.R., B. Taftali, and R. DesRoches, *Seismic performance assessment of steel frames with shape memory alloy connections, Part II–Probabilistic seismic demand assessment.* Journal of Earthquake Engineering, 2010. 14(5): p. 631-645.
[35] Andrawes, B. and R. DesRoches, *Unseating prevention for multiple frame bridges using superelastic devices.* Smart Materials and Structures, 2005. 14(3): p. S60.
[36] Youssef, M., M. Alam, and M. Nehdi, *Experimental investigation on the seismic behavior of beam-column joints reinforced with superelastic shape memory alloys.* Journal of Earthquake Engineering, 2008. 12(7): p. 1205-1222.
[37] Graesser, E. and F. Cozzarelli, *Shape-memory alloys as new materials for aseismic isolation.* Journal of Engineering Mechanics, 1991. 117(11): p. 2590-2608.
[38] Speicher, M.S., *Cyclic testing and assessment of shape memory alloy recentering systems*. 2009, Georgia Institute of Technology.
[39] Renzi, E., et al., *Design, test and analysis of a light-weight dissipative bracing system for seismic protection of structures.* Earthquake engineering & structural dynamics, 2007. 36(4): p. 519-539.
[40] Renzi, E., N. Ranieri, and G. DeCanio. *Experimental verifications of seismic protection of steel and RC structures at Enea-Casaccia shaking tables*. in *Proc., 13th World Conf. on Earthquake Engineering*. 2004.
[41] P. Clark, K. Frank, H. Krawinkler, R. Shaw, Protocol for Farbrication, Inspection, Testing, and Documentation of Beam-Column Connection Tests and Other Experimental Specimens. SAC Steel Project Background Document, 1997.
[42] Ciampi, V., M. De Angelis, and F. Paolacci, *Design of yielding or friction-based dissipative bracings for seismic protection of buildings.* Engineering Structures, 1995. 17(5): p. 381-391.
[43] Wilde, K., P. Gardoni, and Y. Fujino, *Base isolation system with shape memory alloy device for elevated highway bridges.* Engineering structures, 2000. 22(3): p. 222-229.
[44] Christopoulos, C., et al., *Self-centering energy dissipative bracing system for the seismic resistance of structures: development and validation.* Journal of Structural Engineering, 2008. 134(1): p. 96-107.
[45] Miller D.J. *Development and experimental validation of self-centering buckling-restrained braces with shape memory alloy*. M.S. Thesis, University of Illinois at Urbana–Champaign, 2011.
[46] Krawinkler, H., 2000, *State of the Art Report on Systems Performance of Moment Steel Frame Buildings in Earthquakes*, FEMA 355C, Federal Emergency Management Agency, Washington, DC.
[47] Mazzoni, S., et al., *The Open System for Earthquake Engineering Simulation (OpenSEES) User Command-Language Manual.* 2006.
[48] Ibarra, L.F., R.A. Medina, and H. Krawinkler, *Hysteretic models that incorporate strength and stiffness deterioration.* Earthquake engineering & structural dynamics, 2005. **34**(12): p. 1489-1511.
[49] Lignos, D.G. and H. Krawinkler, *A database in support of modeling of component deterioration for collapse prediction of steel frame structures*, in *Structural Engineering Research Frontiers*. 2007. p. 1-12.
[50] Silwal, B., O.E. Ozbulut, and R.J. Michael, *Incremental Dynamic Analyses of Steel Moment Resisting Frames with Superelastic Viscous Dampers*, in *Special Topics in Structural Dynamics, Volume 6*. 2016, Springer. p. 165-174.
[51] Vamvatsikos, D. and C.A. Cornell, *Incremental dynamic analysis.* Earthquake Engineering & Structural 52, 2002. 31(3): p. 491-514.
[52] FEMA, P., *695. Quantification of Building Seismic Performance Factors.* Federal Emergency Management Agency, 2009.
[53] Vamvatsikos, D. and C.A. Cornell, *Applied incremental dynamic analysis.* Earthquake Spectra, 2004. 20(2): p. 523-553.
[54] Venture, S.J. and G.D. Committee, *Recommended seismic design criteria for new steel moment-frame buildings*. Vol. 350. 2000: Federal Emergency Management Agency.
[55] Venture, S.J., *Recommended seismic evaluation and upgrade criteria for existing welded steel moment-frame buildings*. Vol. 351. 2000: Federal Emergency Management Agency.
[56] Ibarra, L., R. Medina, and H. Krawinkler. *Collapse assessment of deteriorating SDOF systems*. in *Proceedings of the 12th European Conference on Earthquake Engineering*. 2002.

Appendix A

The ground motions selected from FEMA P695 are shown in table A1. Also, cross sections of beam and column elements of SAC buildings are listed in Table A2.

Table A1. Details of ground motions used for analysis

ID No.	Earthquake	Year	Magnitude (M_w)	Station	Joyner-Boore Distance (Km)	PGA (g)	PGV (cm/s)
1	Northridge	1994	6.7	Beverly	9.4	0.52	63
2		1994	6.7	Canyon	11.4	0.48	45
3	Duzce	1999	7.1	Bolu	12	0.82	62
4	Hector	1999	7.1	Hector	10.4	0.34	42
5	Imperial Valley	1979	6.5	Delta	22	0.35	33
6		1979	6.5	Elcentro	12.5	0.38	42
7	Kobe	1995	6.9	Nishi	7.1	0.51	37
8		1995	6.9	Shin	19.1	0.24	38
9	Kocaeli	1999	7.5	Duzce	13.6	0.36	59
10		1999	7.5	Arcelik	10.6	0.22	40

Table A2. Cross sections of 3-, 9-, and 20-story buildings

Stories	3-story building			9-story building			20-story building		
	Columns		Girder	Columns		Girder	Columns		Girder
Story 1	W14X159	W14X176	W24X76	W24X229	W24X229	W30X108	W24X229	W24X229	W30X132
Story 2	W14X159	W14X176	W24X84	W24X229	W24X229	W30X116	W24X229	W24X229	W30X132
Story 3	W14X159	W14X176	W18X40	W24X229	W24X229	W30X108	W24X229	W24X229	W30X132
Story 4				W24X229	W24X229	W27X94	W24X229	W24X229	W30X132
Story 5				W24X207	W24X207	W27X94	W24X229	W24X229	W30X132
Story 6				W24X207	W24X207	W24X76	W24X192	W24X192	W30X132
Story 7				W24X162	W24X162	W24X76	W24X192	W24X192	W30X132
Story 8				W24X162	W24X162	W24X62	W24X192	W24X192	W30X116
Story 9				W24X131	W24X131	W24X62	W24X192	W24X192	W30X116
Story 10							W24X192	W24X192	W27X114
Story 11							W24X192	W24X192	W27X114
Story 12							W24X192	W24X192	W27X94
Story 13							W24X192	W24X192	W27X94
Story 14							W24X162	W24X162	W27X94
Story 15							W24X162	W24X162	W27X94
Story 16							W24X162	W24X162	W24X62
Story 17							W24X162	W24X162	W24X62
Story 18							W24X131	W24X131	W21X57
Story 19							W24X131	W24X131	W21X57
Story 20							W24X131	W24X131	W21X57